Integrated Doppler Tracking and Efficient Resampling for Phase-Coherent Acoustic Communication

Abstract

A computationally efficient method for integrating Doppler frequency shift estimation and sample rate interpolation of an acoustic communication signal in a time-varying environment is proposed. The estimation of the Doppler shift is performed using a second-order phase-locked loop in conjunction with the decision-feedback equalizer (DFE). Initial acquisition may be accomplished during the training period of the equalizer so that a separate estimation step is not required. Tracking of the Doppler shift continues in decision-directed mode. Resampling based on the Doppler estimate is performed with a filter bank which is optimized in the least-squares sense for fractionally-spaced sampling. The total computational requirement is proportional to the size of the interpolation filters and the update rate of the interpolator, which is made efficient through use of a pre-computed filter bank. The size of the filters is determined by the SNR required to support a given constellation density and simulation results are presented to demonstrate the performance of the resampler.

Results from in-water testing are included to demonstrate the performance advantage of continuous Doppler tracking in a time-varying environment. Test environments include both shallow and deep-water, rates of 1250-5000 symbols per second, and center frequencies of 2 to 25 kHz. The capability of the method to track Doppler through multiple sign changes is demonstrated with a 60 second long transmission from a circling platform.

Keywords

Doppler shift, acoustic communication, PLL, interpolation, timing recovery, filter bank.

I. Introduction

Relative motion between a source and receiver results in a Doppler-shifted communication signal whose distortion is proportional to the ratio of propagation speed to relative platform speed. In the underwater acoustic channel the propagation speed is low relative to potential source-receiver velocities, leading to time-scale changes which are significantly greater than those encountered at radio frequencies. The magnitude of the time compression or expansion is 0.1% for slow-moving systems, but can potentially reach 1% when two fast-moving underwater vehicles attempt to communicate. The effects vary with time when accelerations due to speed or course changes are present; when both source and receiver are in motion, the resulting acceleration may exceed 1 m/s^2. While UUVs may operate at high speeds, wave-following buoys are subject to accelerations that may reach 4 m/s^2 at sea-state 6. The effects of large time-scale changes will adversely affect the throughput of high-rate, bandwidth-efficient communication unless tracked and removed.

The fractionally-spaced DFE operating on a complex baseband signal with filter coefficients adapted using the minimum mean-square error (MSE) criterion is capable of adjusting its filter taps to compensate for carrier phase offset and jitter [1]. However, as pointed out in [2], relying on the equalizer to correct for carrier phase shift results in excess MSE because the tracking gain must be set higher than if the phase shift were compensated using an explicit tracking loop. While the MSE-adapted filter is

capable of performing time-scale interpolation as well, there are several reasons to consider a separate resampler. The first reason is the same as that which motivates separate carrier phase recovery: an equalizer with tracking rate optimized for ISI removal, phase recovery *and* time-scale interpolation will operate with a higher MSE than an equalizer only tracking ISI. In addition, when the resampling function is performed by the equalizer, the reference tap will eventually move out of the filter window as the symbol timing error slowly grows. While this can be alleviated through use of filter lengths sufficient to span the maximum time compression or expansion, excess MSE and reduced tracking capability may result from the use of needlessly large filters.

The Doppler tracking techniques proposed here draw upon results from phase-locked loop analysis by numerous authors. The PLL design and analysis work in [3] and [2] were incorporated into the single-channel [4] and multi-channel [5] DFE for use in the underwater environment. These receivers were subsequently modified in [6] to improve tracking performance and in [7] to use a single tracking loop for a multi-channel receiver with long feedforward filters. This phase tracking method forms the starting point for the Doppler estimation portion of the receiver described here.

Optimal digital interpolation for band-limited signals is discussed in both [8] and [9]. Additional work presented in [10] and [11] provides background on interpolation methods focused on sample-clock recovery. While this application is slightly different than that in [9] or [11], the analysis of interpolator performance for an over-sampled signal is relevant to the design of baseband digital interpolators for the Doppler-compensation problem. These topic are discussed more completely in Section III.

Several Doppler compensation methods focused on underwater acoustic communication have been proposed. In [6] a method for estimating the Doppler shift at the start of a data packet and then interpolating the entire packet at the same rate was presented. For constant Doppler this technique offers identical performance to that proposed here. Another fixed-estimate approach was reported in [12]. This method measures the time delay between dedicated signals inserted into the data stream and uses the measured temporal expansion or contraction to calculate the interpolation rate. The interpolation is then performed on the block of data between the two measured signals.

A method for estimating the time-varying Doppler of m-sequences used for tomography [13] treats some of the same topics presented here, but the need to operate at a very low symbol SNR lead the authors to develop a heterodyning and low-pass filtering approach which differs significantly from the proposed decision-directed approach.

The contribution of this paper is an efficient Doppler compensation method which operates at the baseband sample rate, requires minimal block-wise processing and offers low-latency. The proposed method is thus suitable for realtime implementation using inexpensive digital signal processors with

limited memory. For typical autonomous vehicle speeds of 1-3 m/s, the DFE training data is used to acquire the Doppler shift, which is then tracked in decision-directed mode for any packet length. No additional timing recovery sequences are required and high-rate Doppler tracking is achieved independent of packet length. When the expected Doppler is high, an additional estimation step may be used to provide an initial starting point for the integrated tracking system.

Through variation of the filter-bank size and filter update rate the residual distortion of the re-sampling process can be modified to suit the SNR of any PSK or QAM constellation. Thus the computational load is optimized to meet an actual fidelity requirement.

The paper is organized as follows: in Section II the model of the Doppler-shifted communication channel is presented. Section III presents the interpolation filter design method and summarizes its performance. In Section IV the PLL, DFE and sample-rate estimation process is discussed. Results of in-water testing are included in Section V.

II. Channel Model

The shallow water channel is modeled by a time-varying impulse response

$$c(\tau, t) = \sum_{p=1}^{P} c_p(t) \delta(\tau - \tau_p(t)) \tag{1}$$

where t denotes the time of observation, and τ denotes the delay. Two phenomena characterize this channel: time spreading and frequency spreading. Time spreading is caused by propagation over multiple paths, distinguished by indices p in the above model. In shallow water, multipath propagation is mainly caused by signal reflections from the surface, bottom and any objects in the water. Reflections that reach the receiver with significant energy determine the total number of paths P needed to represent the channel response. Each path is described by a gain $c_p(t)$ and a delay $\tau_p(t)$. Frequency spreading is caused by the time-variability of these quantities.

For low relative source-receiver speeds, time-variation of the path delays is often neglected. This approximation is justified when signals are transmitted in short packets such that no significant changes in path delays occur over the packet. Consequently, it suffices to design a receiver as if the path delays were constant. The maximum path delay then represents the multipath spread of the channel and serves to determine the size of equalizer filters needed for processing of the high-rate digital signals. Any frequency spreading in this case is caused by the time-variation of the path gains only. An adaptive equalizer will track this time-variation provided that it is slow relative to the data rate. The rate of the channel time-variation is represented by the Doppler frequency spread.

3

Path gains are often modeled as random processes, and described by the second-order statistics:

$$R_p(\Delta t) = E\{c_p(t + \Delta t)c_p^*(t)\}. \tag{2}$$

The Fourier transform of the above autocorrelation function represents the Doppler power spectrum of the random process $c_p(t)$:

$$S_p(\nu) = \int_{-\infty}^{+\infty} R_p(\Delta t)e^{-j2\pi\nu\Delta t}d\Delta t. \tag{3}$$

The bandwidth of this function is the Doppler spread which quantifies the frequency spreading of the signal traveling on the pth path. The shape of the Doppler spectrum depends on the model used to represent the randomly time-varying path gains.

In mobile underwater communication systems, explicit motion between the transmitter and receiver introduces additional time-variation of the channel. This time-variation becomes a dominant factor in determining the frequency spreading properties of the channel when mobile units are moving at speeds of several m/s. At such speeds, changes in the propagation path length that occur in one data packet cannot be neglected. Consequently, it is no longer possible to neglect the time-dependence of the path delays. Time-variability of the path delay causes the time dilation or compression of the signal which must be taken into account when designing a receiver.

A simple model for the time-dependence of the path delay can be obtained by considering receiver-transmitter motion at a constant relative speed v. The resulting Doppler spread will be a function of the speed v normalized by the speed of sound c. The exact functional dependence is related to the statistical model of the entire scattering process.

Nevertheless, it is always possible to develop a simplified model, without any statistical assumptions, to provide at least an insight into the Doppler spreading process caused by the receiver/transmitter motion. To do so, let us consider transmission of a signal $s(t)$, which represents a baseband signal $u(t)$ modulated onto a carrier of frequency $f_c = \omega_c/2\pi$

$$s(t) = Re\{u(t)e^{j\omega_c t}\}. \tag{4}$$

Relative motion between the transmitter and receiver results in the variation of the path length traveled by the signal. Let us consider a single propagation path, and let the distance between the transmitter and the receiver at time t_0 be l_0. The signal received at time t_0 is then equal to the signal that was transmitted l_0/c seconds earlier:

$$r(t_0) = s(t_0 - l_0/c). \tag{5}$$

At a subsequent time instant, $t_0 + \Delta t$, the receiver has moved away from the transmitter so that the distance between them is now $l_0 + l$. Since the relative speed of this motion is v, the distance traversed

during Δt is $l = v\Delta t$. (There is no loss of generality in assuming a different direction of the motion.) Hence, the signal received at time $t_0 + t$ is equal to the signal transmitted $(l_0 + l)/c$ seconds earlier:

$$r(t_0 + \Delta t) = s(t_0 + \Delta t - (l_0 + v\Delta t)/c) \tag{6}$$

Setting $t_0 + \Delta t = t$, the received signal can be expressed in terms of a time-varying delay $\tau(t)$ as

$$r(t) = s(t - \tau(t)) \tag{7}$$

where

$$\tau(t) = \tau_0 + vt/c \tag{8}$$
$$\tau_0 = l_0/c - vt_0/c \tag{9}$$

Alternatively, the received signal can be expressed as

$$r(t) = s(at - \tau_0) \tag{10}$$

where

$$a = 1 - v/c \tag{11}$$

is the time-scaling factor (a plus sign would result if we considered the receiver and transmitter moving towards each other).

To distinguish the effects of Doppler spreading and Doppler shifting, it is insightful to look at the equivalent baseband representation of the received signal:

$$r(t) = Re\{v(t)e^{j\omega_c t}\}. \tag{12}$$

Upon substituting for the signal $s(t)$ in terms of its baseband equivalent $u(t)$ in the expressions for the received signal $r(t)$, it is found that

$$v(t) = u(at - \tau_0)e^{j\phi_0}e^{j2\pi f_{dv}t} \tag{13}$$

where $\phi_0 = \omega_c\tau_0$ is the constant phase offset, and $f_{dv} = -f_c v/c$ is the Doppler shift. The carrier frequency thus appears shifted at the receiver by the amount $f_{dv} = \omega_{dv}/2\pi$. The Doppler spread is caused by time-scaling, as described by the factor $a \neq 1$. The frequency occupancy of the received signal is evident from the Fourier transform of the baseband equivalent $v(t)$:

$$V(f) \sim U((f - f_{dv})/a). \tag{14}$$

Thus an input baseband signal of bandwidth B centered around 0 Hz is observed at the receiver (after nominal carrier demodulation) as a signal of bandwidth aB (Doppler spreading) centered around f_{dv} Hz (Doppler shifting).

Motion-induced Doppler spreading and shifting are hence both characterized by the factor v/c. Unlike in the case of radio communications, where this factor is at most on the order of 10^{-7} (for a vehicle speed of 100 km/h), in an underwater acoustic scenario, it is on the order of 10^{-2} for vehicle speeds of about 5 m/s. As a consequence, the time-scaling effect is not negligible in an underwater acoustic mobile system. It should be noted that in a realistic scenario, the relative speed v will be varying in time. Consequently, the Doppler spread calculated above can only be regarded as an instantaneous value, i.e. as one among a range of values that the true spreading (and shifting) will be assuming in time. Also, depending upon the geometry of the channel, different propagation paths will experience different frequency spreading.

III. Efficient Time-Varying Interpolation

The fractional sampling-rate deviation caused by Doppler shift is difficult to correct using the conventional re-sampling technique, i.e., interpolation by an integer factor m, followed by decimation by another factor, n. This method adjusts the input sampling rate by a factor m/n and thus to achieve a small sampling-rate change, n and m must be large (e.g., for a -0.5% change equivalent to a differential Doppler velocity of 7.5 m/s, m and n would be 199 and 200, respectively). A computationally expensive filtering operation is required at the high intermediate sampling rate, mf_b, where f_b is the baseband sampling rate, making this method impractical.

A second approach resamples the input signal using a time-varying interpolating filter. For a fractional sampling rate variation of $\delta = v/c$ (which may be time-varying), the output samples from the resampler are, ideally: s_k, $s_{k+1+\delta}$, $s_{k+2+2\delta}$,..., where s_k, s_{k+1},... are the input samples and the fractional index $n\delta$ implies interpolation between the neighboring points in s_k. The output samples can be approximated by interpolating by, successively, $\delta, 2\delta, 3\delta, ...$ on a sliding window of the input signal. For an r-tap interpolating filter, the computational cost of this method is approximately rf_b multiplications per second plus the cost of generating a new interpolating filter for each output sample. Interpolating filters can be computed iteratively, or selected from a look-up-table. Iterative computation has the advantage of producing an interpolator giving the exact phase lag required but is restricted by complexity considerations to short interpolation filters which may introduce some spectral distortion and noise. The look-up-table method allows the use of longer filters but requires an approximation in phase lag due to the limited number of filters to choose from.

A method combining the virtues of each of these approaches has been developed to reduce computational effort and memory usage while minimizing spectral distortion in the signal band. The algorithm includes a method for computing optimal interpolating filter tables and a fast method for interpolating between filters in the look-up table to permit the use of a small filter bank. In addition, the effect of updating the filters at a rate less than the symbol rate is examined as a means of reducing computations.

A. Time-Delay Filter Design

There are two key components in the interpolator. The first is an accumulator used to determine the fractional time delay $\tau(i) = \sum_{i=1}^{n} \delta(i)$ required for the next output sample. The second component in the interpolator is an algorithm for computing filter coefficients for a given time delay. This algorithm produces filters from an underlying filter family, selected to provide a satisfactory trade-off between computational burden and resampling noise (i.e., noise due to spectral distortion by the filter). An example of a time delay filter is the sinc function. There are many other possible filter families and the selection of a suitable family will be discussed below.

In a coherent acoustic communications receiver, a fractionally-spaced equalizer is often used to provide accurate timing alignment. This implies an input sampling rate of $f_b = 2/T$ Hz. However, the signal energy is constrained to $\pm 1/2T$ Hz. It is only necessary for the resampler to provide accurate Doppler correction at frequencies up to half the symbol-rate, i.e., about one-quarter of the input sampling-rate. This suggests that a frequency-weighted approach to time-delay filter design can be used to achieve optimal performance from short, computationally-efficient, filters.

The desired frequency response of a time-delay filter is $D(e^{j\omega}) = e^{-j\tau\omega}$, where τ is the filter time delay in fractions of a sample. As noted above, this need only be maintained accurately over the frequency range $-\omega_0 < \omega < \omega_0$, where ω_0 is the upper frequency limit ($2\pi f/f_b$ radians per sample) of the signal of interest. The bandlimited mean-square-error between the desired and actual filter responses is defined as

$$\gamma = \int_{-\omega_0}^{\omega_0} |D(e^{j\omega}) - H(e^{j\omega})|^2 d\omega \tag{15}$$

where $H(e^{j\omega})$ is the frequency response of the candidate filter. Using an FIR filter realisation with n samples of causal support, the time-delay filter has a $2n+1$-coefficient real vector $H = [h_{-n}, \ldots, h_0, \ldots, h_n]^T$ and $H(e^{j\omega}) = H^T W$, where $W = [e^{-jn\omega}, \ldots, 1, \ldots, e^{jn\omega}]^T$. The filter coefficients minimizing γ can be determined by differentiating (15) with respect to H and setting $d\gamma/dH = 0$. The derivative of H is

$$\frac{d\gamma}{dH} = \int_{-\omega_0}^{\omega_0} \{2WW^H H - 2\mathrm{Re}(e^{j\tau\omega}W)\}d\omega \tag{16}$$

7

where W^H denotes the conjugate transpose. Setting the result to 0 yields

$$H = \left(\int_{-\omega_0}^{\omega_0} WW^H d\omega \right)^{-1} \mathrm{Re} \left(\int_{-\omega_0}^{\omega_0} e^{j\tau\omega} W \right) d\omega. \tag{17}$$

Defining

$$R = \int_{-\omega_0}^{\omega_0} WW^H d\omega \tag{18}$$

and

$$P = \mathrm{Re} \left\{ \int_{-\omega_0}^{\omega_0} e^{j\tau\omega} W d\omega \right\} \tag{19}$$

(17) becomes the familiar least-squares solution

$$H = \mathbf{R}^{-1}P \tag{20}$$

where

$$\mathbf{R} = 2 \begin{bmatrix} \omega_0 & \sin\omega_0 & \frac{1}{2}\sin 2\omega_0 & \cdots \\ \sin\omega_0 & \omega_0 & \sin\omega_0 & \cdots \\ \frac{1}{2}\sin 2\omega_0 & \sin\omega_0 & \omega_0 & \cdots \\ \vdots & \vdots & \vdots & \ddots \end{bmatrix} \tag{21}$$

and

$$P = 2 \begin{bmatrix} \frac{\sin(\tau-n)\omega_0}{\tau-n} \\ \vdots \\ \frac{\sin\tau\omega_0}{d} \\ \vdots \\ \frac{\sin(\tau+n)\omega_0}{\tau+n} \end{bmatrix}. \tag{22}$$

Only P is dependent on the time delay, τ, and so for a given filter length, only one matrix inversion is necessary to compute the entire filter bank.

For the degenerate full-band case $(\omega_0 = \pi)$, $\mathbf{R} = \pi\mathbf{I}$ and $P = \pi[\mathrm{sinc}(\tau - n), \ldots, \mathrm{sinc}(\tau), \ldots \mathrm{sinc}(\tau + n)]^T$, where $\mathrm{sinc}(x) = \sin(\pi x)/\pi x$. In this case the least-square interpolator is identical to the sinc function interpolator and thus the sinc function interpolator is the optimal full-band interpolator using the criteria in (15).

B. Time-Delay Filter Bank

The least-squares filter computation algorithm of (20) requires $(2n + 1)^2$ operations per filter (assuming that $\mathbf{R}$ is inverted off-line), making it unsuitable for real-time computation. A better strategy is to pre-compute a range of time-delay filters and select the closest to the required time-delay at each sample. For a given filter bank size, two techniques can be used to improve accuracy.

The first technique exploits the inherent symmetry in the time-delay filters to minimize the range of filters needed in the filter bank. This follows from the observations that (i) a negative time delay

8

of τ samples can be realized by reversing the coefficients of a positive τ time-delay filter, and (ii) a time-delay > 0.5 can be realised by a unit-sample shift and a negative time-delay filter of $\tau - 1$ samples. Exploiting these facts, it is only necessary to have time delays of between 0 and 0.5 samples represented in the filter bank allowing finer resolution for a fixed-size bank.

The second technique for improving accuracy is to interpolate between filters in the filter bank. Using first-order interpolation the time-delay filter for a desired delay τ is approximated as

$$H(t) = H(\tau_0) + \frac{\tau - \tau_0}{\tau_1 - \tau_0}(H(\tau_1) - H(\tau_0)) \tag{23}$$

where τ_0 and τ_1 are the two flanking time delays represented in the filter bank. The computation burden of (23) can be reduced by pre-computing the scaled difference filter bank:

$$G(\tau_i) = \frac{1}{\tau_{i+1} - \tau_i}(H(\tau_{i+1}) - H(\tau_i)) \tag{24}$$

for $i = 0, \ldots, 2n + 1$. Using (24), (23) simplifies to

$$H(\tau) = H(\tau_0) + (\tau - \tau_0)G(t_1). \tag{25}$$

To summarize, for an m-filter bank at a time delay of τ samples:

1. Subtract or add 1 to τ until $-0.5 < \tau < 0.5$. Shift the filter window right (left) for each subtraction (addition).

2. Find the closest time delay to $|\tau|$ represented in the filter bank.

3. Interpolate using (25) ($2n + 1$ operations).

4. Reverse the filter if τ is negative.

C. Filter Update Rate

The time-delay filter generated using the approach described above does not need to be updated for each output sample. The same time-delay filter can be used for 10 to 50 samples with only a small increase in resampling noise. This significantly reduces the computation time needed for the filter selection portion of the resampling algorithm.

The performance of the interpolater with respect to filter lengths from 3 to 15 and update rates from 2 to 60 points is shown in Fig. 1. The frequency weighting is set to 0.5 of Nyquist (i.e. $\omega_0 = \pi/2$) in this case. The noise level for different filter lengths with respect to update period is computed by measuring the error at each frequency and then integrating the resulting noise in the communication band using the spectrum of the raised-cosine function with $\alpha = 0.5$.

9

The filter length and update period for a given density constellation can be selected based on this analysis. BPSK and QPSK modulation require only short filters and infrequent updates, while 16-QAM requires a 9-15 length filter with frequent updating. Thus the computational requirements of the resampling system may be matched to a particular PSK or QAM constellation size.

IV. The Receiver

The receiver is a multi-channel decision feedback equalizer (DFE) with 2nd order phase-locked loop (PLL) [4] equipped with the time-varying interpolator described in Section III and shown in Fig. 2. While the receiver described in [4] employs one PLL per input channel, here a phase estimate $\hat{\theta}(i)$ from a single PLL, is applied to the composite symbol estimate from all channels [7]. The measured phase shift is assumed to be dominated by motion-induced Doppler shift rather than local oscillator differences,.

Let the complex baseband signal be represented by $y(i)$ and let the current estimate of the sample-rate error be $\delta(i) = v(i)/c$, where $v(i)$ is the current relative speed between source and receiver. For simplicity of presentation a $1/T$-rate single-channel version of the DFE will be considered. Extensions to the fractionally-spaced multi-channel case are shown in [4] and [6].

The discrete signal $y(i)$ is resampled using the length P interpolation filter H_i generated using (25). The filter H_i is computed using the cumulative delay in symbols at symbol i given by the recursive equation:

$$\tau(i) = \tau(i-1) + \delta(i). \tag{26}$$

The ith time-scale corrected symbol is then computed as

$$x(i) = \sum_{k=1}^{P} H_i(k) y(i + m - P/2 + k - 1)$$

where m is the positive or negative integer portion of $\tau(i)$ which shifts the interpolating filter window to track the change in time scale. The resampled signal, the previous hard decisions $\tilde{d}$ and the phase estimate $\hat{\theta}(i)$ from the PLL are used to update the equalizer and compute the current symbol estimate

$$\hat{d}(i) = \Phi^*(i) W(i) e^{-j\hat{\theta}(i)}$$

where $\Phi(i) = [x(i), x(i-1), \ldots, x(i - N_f - 1), \tilde{d}(i-1), \ldots, \tilde{d}(i - N_b)]$, N_f is the number of feedforward taps and N_b is the number of feedback taps.

The feedforward and feedback filter coefficients in $W(i)$ are jointly-updated using an algorithm from the RLS or LMS families [7] and the symbol error is computed using

$$e(i) = \tilde{d}(i) - \hat{d}(i),$$

where $\tilde{d}$ is the hard decision associated with the current symbol estimate. The phase estimate $\hat{\theta}(i)$ is computed as shown in [4] or [6], then low-pass filtered prior to use in updating the time-shift $\tau(i)$.

First, the instantaneous Doppler shift frequency f_{dv} is estimated from the slope of smoothed phase estimate $\theta'(i)$:

$$f_{dv}(i) = \frac{1}{2\pi T}(\theta'(i) - \theta'(i-1)).$$

11

The fractional Doppler shift factor $\delta(i) = v(i)/c$ is then computed using the carrier frequency f_c:

$$\delta(i) = v(i)/c = f_{dv}(i)/f_c.$$

This value is used in (26), completing the outer, interpolating, loop in the receiver.

The operation of the equalizer is as described in [4], with the exception that the PLL is also used to estimate the Doppler shift frequency and from it the resampling rate via the outer feedback loop. During the equalizer training period the phase and Doppler shift are acquired simultaneously. While normally $\tau(0)$ is initialized to 0, if an estimate of the Doppler shift at the start of a packet is available (e.g. computed as described in [6]), then $\tau(0)$ may be initialized to this value which will reduce the number of symbols required for acquisition.

The total number of computations required to generate the time-scale estimate is very small. Thus this approach, when combined with the interpolation filter update method of Section III, provides an extremely efficient way of removing the time-dilation or compression from phase-coherent signals.

V. Results

The DFE with integrated Doppler estimation and resampling was tested in a number of acoustic channels using different data rates and carrier frequencies. Data from the experiments are used to demonstrate the performance improvement due to the new technique, with and without the use of an initial Doppler estimate. Four test cases are discussed: (A) 1250 symbol per second QPSK at 2.25 kHz, (B) 5000 sps 8-PSK at 15 kHz, (C) 5000 sps QPSK at 25 kHz, and (D) 4000 sps BPSK at 15 kHz. Cases A, B and D are single packet performance examples, while case C includes over one hundred packets at a variety of relative speeds and ranges.

A. 1250 sps at 2.25 kHz Carrier

The first case is from a test carried out in 1996 on the New England continental shelf in 150 m deep water at 6 km range [16]. This test is of interest because it includes a constant relative speed of 2.2 m/s plus a smaller time-varying component. The channel delay-spread (Fig. 3) is almost 0.1 s, but the SNR is high and the multi-channel equalizer provides an output SNR greater than 20 dB. The carrier phase recovered by the PLL after the initial shift has been removed is shown in Fig. 4. The PLL output contains a small linear trend plus a sinusoidal component. The slope of the phase corresponds to a slight error in the initial estimate (0.2 Hz), while the 1 Hz sinusoidal signal is due to motion of the source tow-body. This Doppler change within the data packet will increase the MSE unless it is estimated continuously and removed.

The MSE for three different receivers is shown in Fig. 5. The equalizer with 2nd order PLL, but without Doppler estimation or resampling, yields an average MSE of -10 dB. If the signal is resampled using the Doppler estimated at the start of the packet the average MSE decreases to -22 dB.

The equalizer with integrated resampling provides another 2 dB improvement in MSE by compensating for the change within the packet. The performance difference between the fixed and integrated resampling receivers depends upon the change in Doppler relative to that estimated at the start of the packet. As shown in Fig. 5 the instantaneous performance difference can be as much as 5 dB.

In this particular case the performance difference between the Doppler-tracking equalizer with and without initial estimation is nearly zero; this is because the overall shift is small (3.4 Hz, which corresponds to 2.2 m/s) The PLL acquires and tracks this relatively low carrier frequency offset without introducing additional noise.

B. 5000 sps, 15 kHz Carrier, 8-PSK

A deep-water vertical acoustic communication link from a bottom instrument to a ship or buoy experiences Doppler shifts due to platform motion induced by surface waves. Even moderate sea-states may generate vertical speeds of 1 m/s, depending upon the response of the platform. A test conducted in 3000 m water using 5000 sps 8-PSK modulation (15000 bps) demonstrates the fast rate of change due to surface wave motion. In Fig. 6 the phase recovered by the PLL is shown along with the corresponding time-dilation (compression) factor. For this case the resampling rate changes quickly and constantly throughout the 1.4 s packet, with a maximum sample-rate change of 0.1%. The performance with adaptive resampling is 3 dB better than without resampling.

While the feedforward filter of the DFE can perform some resampling, as the time delay τ increases through the packet, the signal will appear to move through the feedforward filter, causing the equalizer to fail when the delay moves too far. This movement is illustrated in Fig. 7 (top), where the feedforward taps follow $\tau(i)$ in the uncompensated case. This packet is relatively short and the feedforward filters are set wide enough, so that by the end of the packet τ is still less than the feedforward filter width. Adaptive resampling adjusts the reference point of the equalizer to track the delay and maintain symbol synchronization (bottom of Fig. 7). This has the additional benefit of requiring the feedforward filters to span only the channel delay spread, in this case 6 taps. In the un-compensated case 20 taps are necessary, increasing the computational requirement and slowing the adaptation rate.

C. 5000 sps at 25 kHz Carrier

To demonstrate the performance of the equalizer with integrated Doppler estimation and resampling over a wide range of operating conditions the receiver was tested on a large data set where both range and Doppler vary. The track of the source and receiver are shown in Fig. 8, and the relative velocity and range between source and receiver are shown in Fig. 9. This test was performed in water approximately 150-200 m deep on the New England Continental Shelf. The data packets are about 7500 symbols long (1.5 s).

The data from this test have a number of different characteristics due to the variety of maneuvers the source vessel performed. In certain cases the Doppler (whether low or high) is constant throughout the packet, while in other cases the Doppler varies significantly from the initial estimate. The performance improvement of the proposed technique depends upon the Doppler change and whether or not the initial estimate is used. When the initial Doppler estimate is used the required phase-locked loop gain is lower and the error due to tracking lag reduced.

Each data packet is processed three different ways: (a) using an initial Doppler estimate but without

continuous tracking, (b) using the initial estimate plus continuous tracking, and (c) direct acquisition of the initial Doppler shift during training then continuous tracking. The results are summarized in Fig. 10 where the difference in SNR at the output of the equalizer for the receivers with integrated resampling are plotted with respect to the receiver with fixed resampling.

The resampling receiver initialized with an externally-obtained Doppler estimate produces the best overall performance when the relative source-receiver speed is high. As shown in Fig. 10, this receiver is up to 4 dB better than the receiver without integrated tracking and resampling. In general, the greater the Doppler change over a data packet, the greater the gain. However, a few packets begin and end with similar Doppler shift so that the Doppler change from start to end is very small. In these cases the performance improvement is a function of the maximum variation.

The receiver with integrated resampling that does not use the initial Doppler estimate also offers a significant performance improvement as the Doppler change increases, but suffers a slight loss in MSE with respect to the fixed resampling rate receiver when the Doppler change is small. The MSE loss, which averages less than one-half dB, is due to the higher PLL gain necessary to acquire and track the carrier phase shift, and the additional noise that this introduces.

D. 4000 sps at 15 kHz Carrier

The final case is used to demonstrate that the proposed equalizer allows the source and receiver to move arbitrarily with respect to each other including changing the sign of the relative Doppler shift, all within a single data packet. The signal used for the test is 4000 sps BPSK transmitted at a 15 khz carrier with a duration of 60 s (250 000 symbols). This test demonstrates that the receiver can operate continuously through a range of Doppler shifts without the need for additional training or other overhead within the data packet.

The source is rigidly mounted below a small boat and transmits to a fixed, multi-channel receiver. The small boat was turned in tight circles a few hundred meters from the receiver as shown in Fig. 11. One and a half revolutions of a 25 m circle are performed at a speed of 2 m/s. This is similar to the turning rates of small underwater vehicles.

At $t = 0$ the source is starting a turn toward the receiver at 0.7 m/s. The receiver acquires the Doppler shift during the training period without use of an external estimate. As the turn progresses the relative speed increases to a maximum at $t = 10$ s, then decreases until the sign of the Doppler shift changes at $t = 20$ s. The resampling filters automatically switch from time-expansion to time-compression as the source goes from closing range to opening. Another sign change occurs at $t = 40$ s as the transmitter turns toward the receiver again.

Throughout the 60 s the PLL maintains lock on the carrier phase and provides the resampler with time-scale updates. The conventional receiver without integrated resampling fails soon after the packet starts because of the continuous change in the apparent signal rate.

VI. Conclusion

The time-varying Doppler shift caused by changes in relative source-receiver motion creates a sample-rate error that decreases the performance of a phase-coherent receiver. The phase-locked loop operated in conjunction with the DFE provides a frequency offset estimate which may be used to compute the instantaneous sample-rate error and the cumulative delay. Only a few extra computations per symbol are required.

The method does assume that the carrier phase difference is entirely due to motion, not local oscillator differences between source and receiver. Fortunately, clock error and drift are limited to a very small fraction of typical Doppler shifts even with inexpensive crystal oscillators. Small errors in the frequency estimation create small errors in the interpolation filters which has limited impact on overall receiver performance.

The over-sampled signal used by phase-coherent acoustic receivers in the underwater channel limits the required frequency response of an interpolation filter. Taking advantage of the this fact leads to a frequency-weighted filter design approach which may be solved by minimizing the band-limited mean-square error. The least-squares optimal interpolation filter is set for a particular constellation density by adjusting the filter length and its update rate. The BPSK and QPSK signals, which are the most common used for undersea acoustic communication, require filters of only 3 baseband points with filter updates only every 50 samples. A small filter look-up table and a companion difference table used for filter interpolation minimize the number of computations necessary to generate a resampling filter.

The method works well for both fast, constant Doppler (straight-line ship motion), or time-varying Doppler (turning vehicles or vertical wave motion). Acquisition performance at speeds faster than several meters per second may be improved by use of an initial Doppler estimate obtained by any number of methods including those described in [6] and [12]. The result is a scalable approach to Doppler compensation suitable for a wide range of data rates and nearly arbitrary platform motion, all without any changes in the transmitted signal.

References

[1] G. Ungerboeck, "Adaptive maximum likelihood receiver for carrier modulated data transmission system," *IEEE Tr. Comm*, vol. 22, pp. 624-634, 1974.

[2] S. Prasad and S. Pathak, "On jointly adaptive decision feedback equalization and carrier recovery in digital communication systems," *AEÜ*, vol. 43, pp. 135-143, 1989.

[3] D. Falconer, "Jointly adaptive equalization and carrier recovery in two dimensional digital communication systems," *Bell Syst. Tech. J.*, vol. 55, pp. 317-334, Mar. 1976.

[4] M. Stojanovic, J. Catipovic and J. Proakis, "Phase coherent digital communications for underwater acoustic channels", *IEEE J. Oceanic Eng.*, Vol. OE-16, pp. 100-111, Jan. 1994.

[5] M. Stojanovic, J. Catipovic and J. Proakis, "Adaptive multi-channel combining and equalization for underwater acoustic communications", *J. Acoust. Soc. Am.*, **94**, (3), part 1, pp. 1621-1631.

[6] M. Johnson, L. Freitag and M. Stojanovic, "Improved Doppler tracking and correction for underwater acoustic communication," *Proc. ICASSP '97*, vol 1, pp. 575-578, Munich, Germany, April, 1997.

[7] L. Freitag, M. Johnson and M. Stojanovic, "Efficient equalizer update algorithms for acoustic communication channels of varying complexity," *Proc. Oceans '97*, pp. 580-585, Oct. 1997.

[8] G. Oetken, T. Parks and H. Schüssler,"New results in the design of digital interpolators," *IEEE Tr. ASSP*, vol. 23, No. 3, June 1976, pp. 301-309.

[9] D. Kim, M. J. Narasimha and D. C. Cox, "Design of optimal interpolation filter for symbol timing recovery," *IEEE Tr. Comm.*, vol. 45, No. 7, July 1997, pp. 877-884.

[10] F. M. Gardner, "Interpolation in digital modems–part I: fundamentals," *IEEE Tr. Comm.*, vol. 41, No. 3, March 1993, pp. 501-507.

[11] L. Erup, F. M. Gardner and R. Harris, "Interpolation in digital modems–part II: implementation and performance," *IEEE Tr. Comm.*, vol. 41, No. 6, June 1993, pp. 998-1008.

[12] B. S. Sharif, J. Neasham, O. R. Hinton and A. E. Adams,"A computationally efficient Doppler compensation system for underwater acoustic communication," *IEEE J. Oceanic Eng.*, Vol. OE-25, pp. 52-61, Jan. 2000.

[13] I. Schumacher and G. J. Heard, "Removal of time-varying Doppler using phase tracking with application to ocean warming measurements," *J. Acoust. Soc. Am.*, **96** (3), Sept. 1994, pp. 1805-1812.

[14] L. Brekhovskikh and Y. Lysanov, *Fundamentals of Ocean Acoustics*, New York: Springer, 1982.

[15] T. Rappaport, *Wireless Communications: Principles and Practice*, Upper Saddle River, NJ: Prentice Hall, 1996.

[16] L. Freitag, M. Johnson, M. Stojanovic, D. Nagle and J. Catipovic, "Survey and analysis of underwater acoustic channels for coherent communication in the medium-frequency band," *Proc. Oceans 2000*, Providence, Sept. 2000.
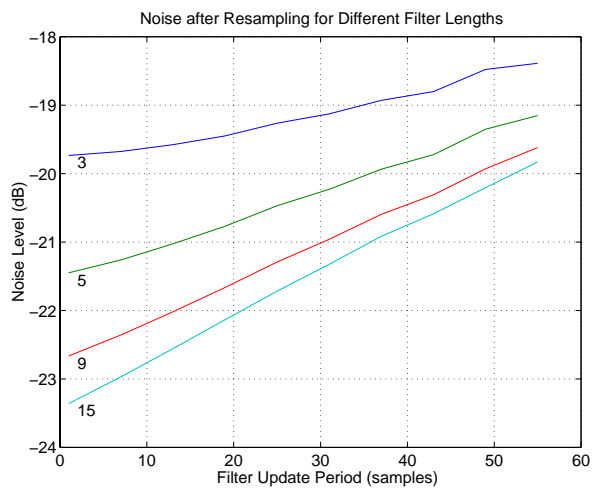
Fig. 1. Interpolation filter performance with fractional sampling.
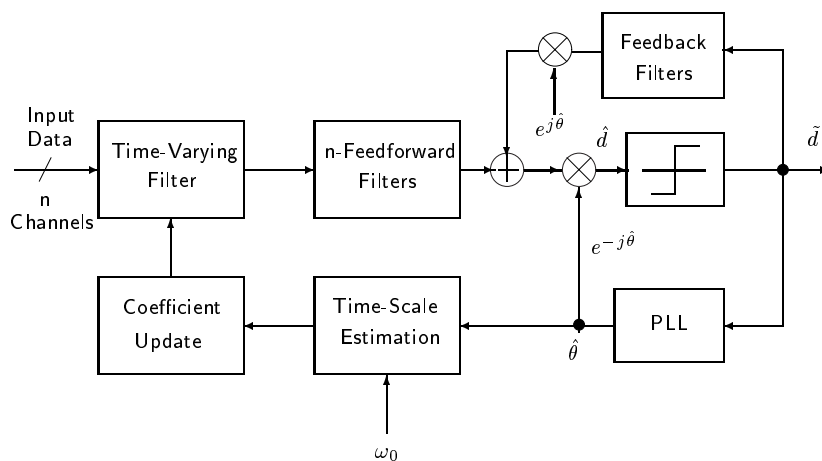
Fig. 2. Receiver block diagram.
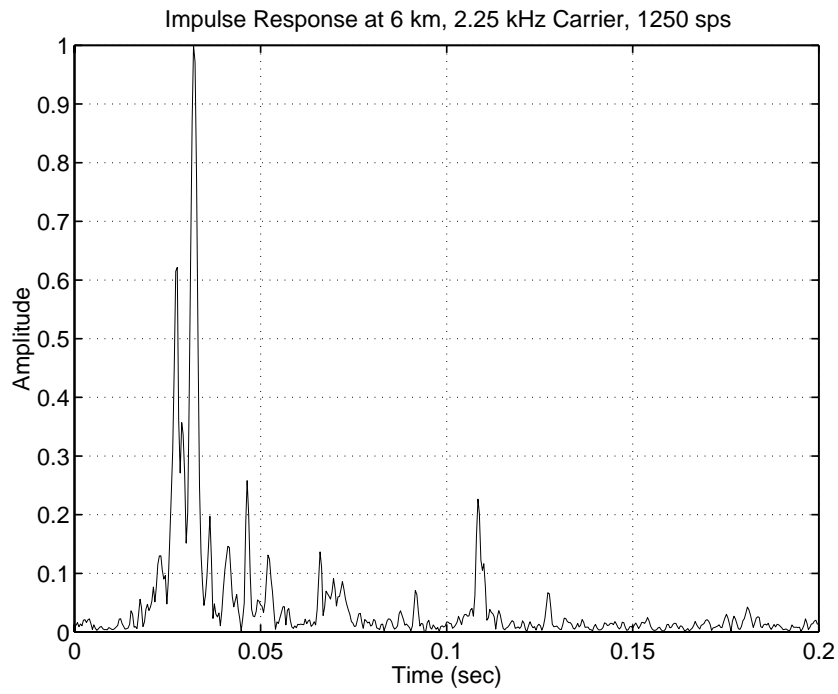
Fig. 3. Impulse Response for Case A.

Fig. 4. Phase for Case A.

Equalizer MSE. (A) No compensation (B) Single Estimate (C) Integrated
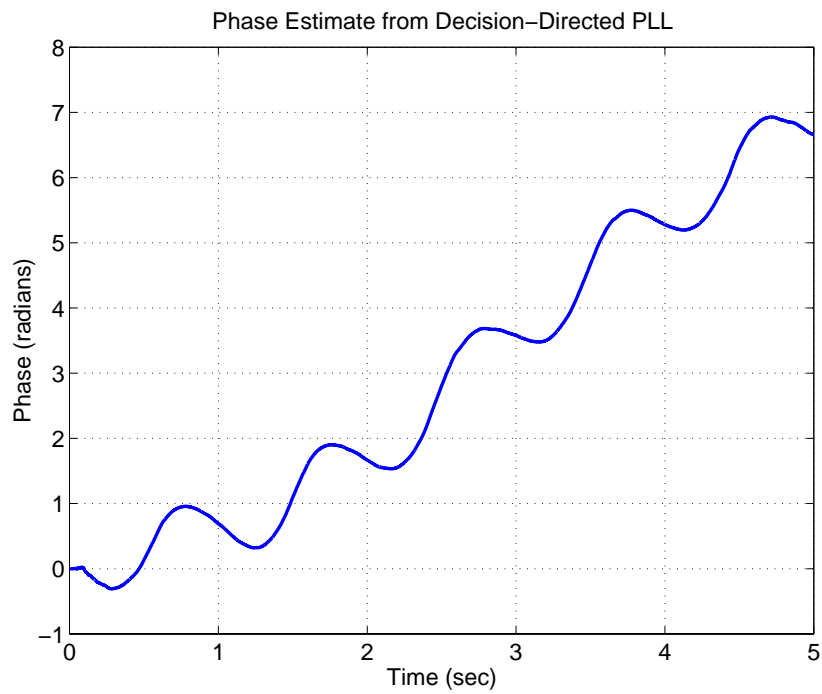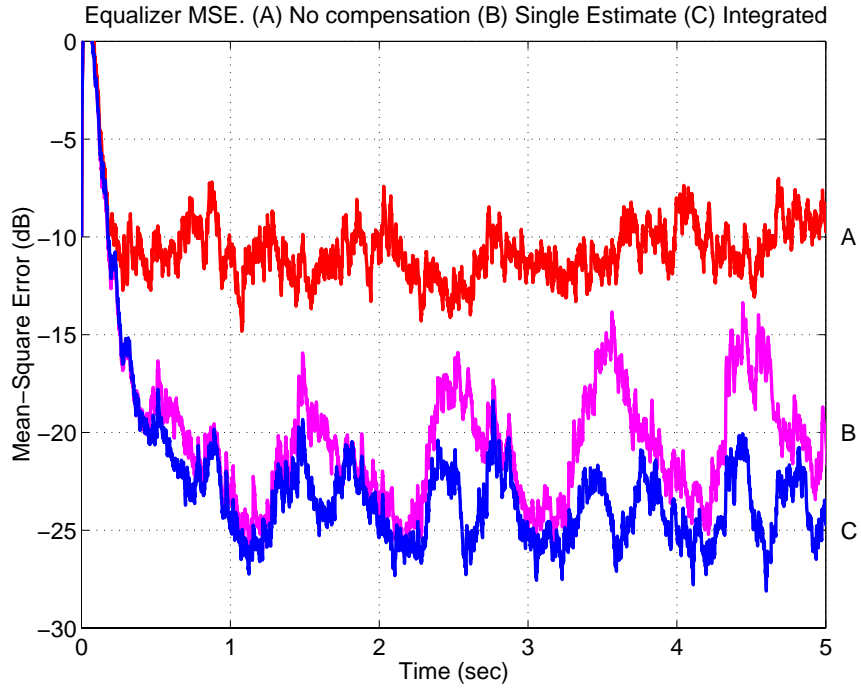
Fig. 5.   Equalizer MSE for Case A processed three different ways. (A) No resampling. (B) Resampled based on an estimate obtained at the start of the packet. (C) Continuously estimated and resampled.
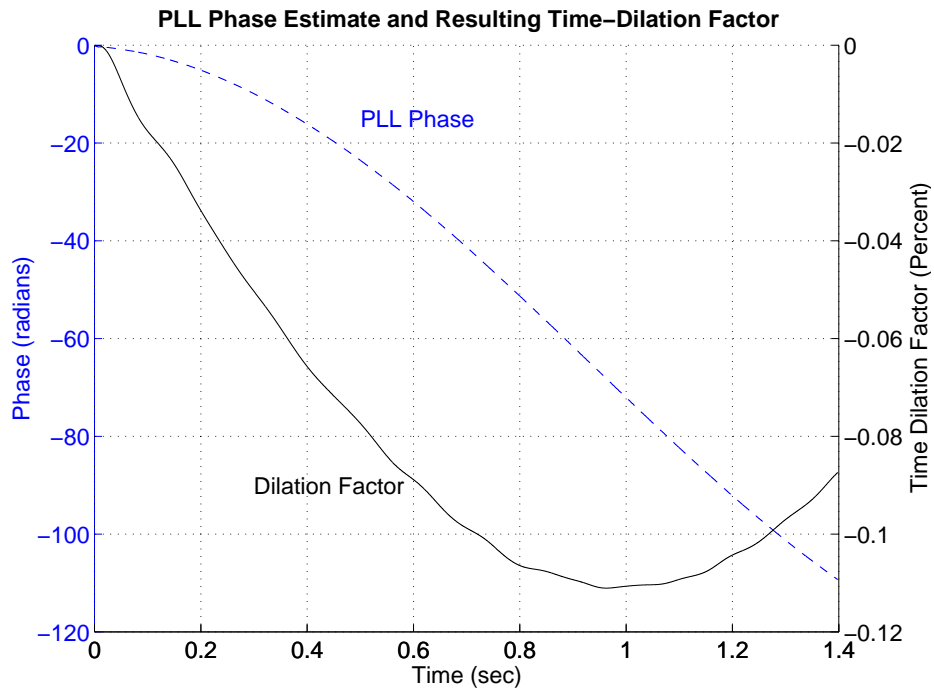
Fig. 6.   Vertical channel phase and time-dilation factor due to surface heave for Case B.

Feedforward Tap Evolution: No Doppler Tracking

Feedforward Tap Evolution: With Doppler Tracking
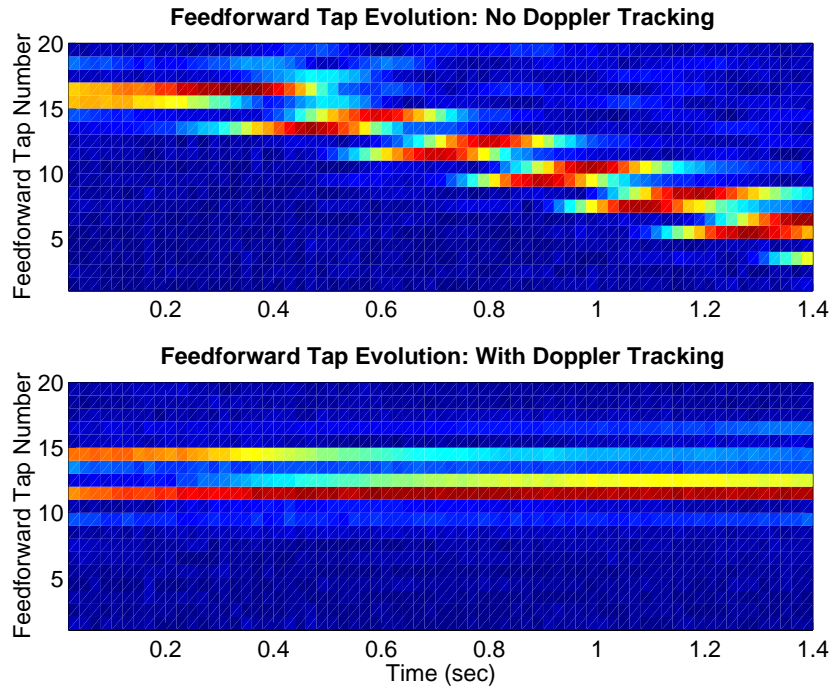
Fig. 7. Feedforward tap magnitude for vertical channel communications without integrated Doppler tracking and resampling (top), and with integrated processing (bottom).

Source and Receiver Tracks
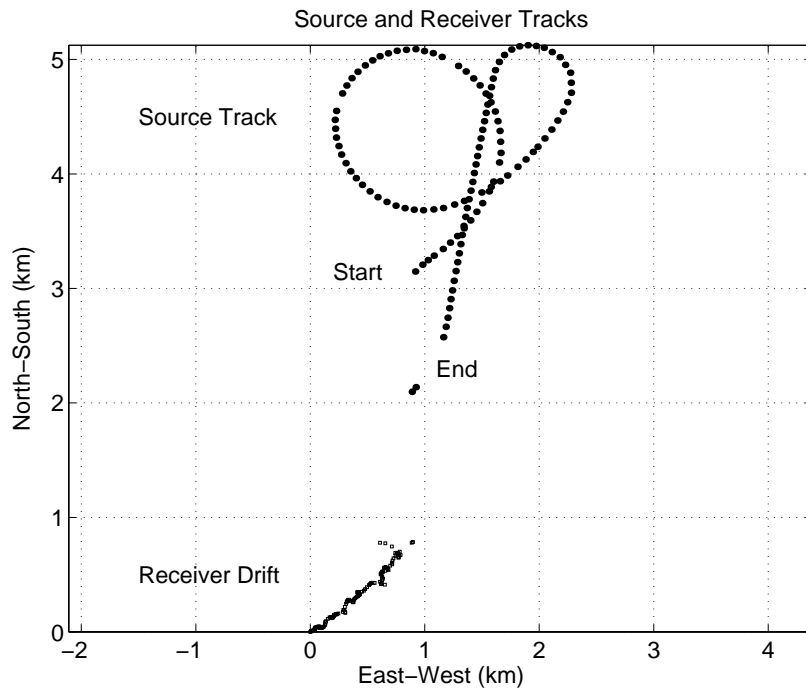
Fig. 8. Source-receiver test tracks for Case C.
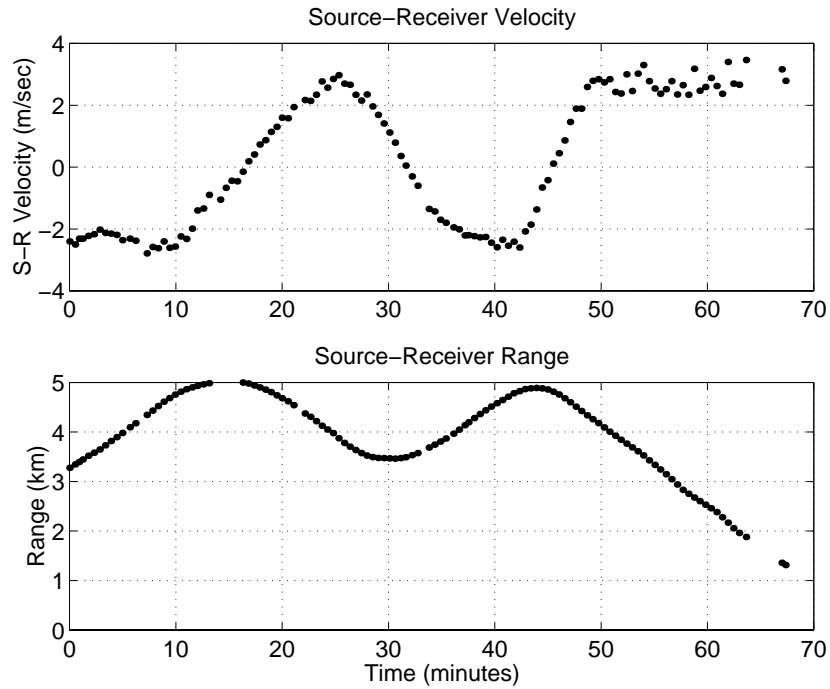
Fig. 9.   Velocity and range between source and receiver for Case C.
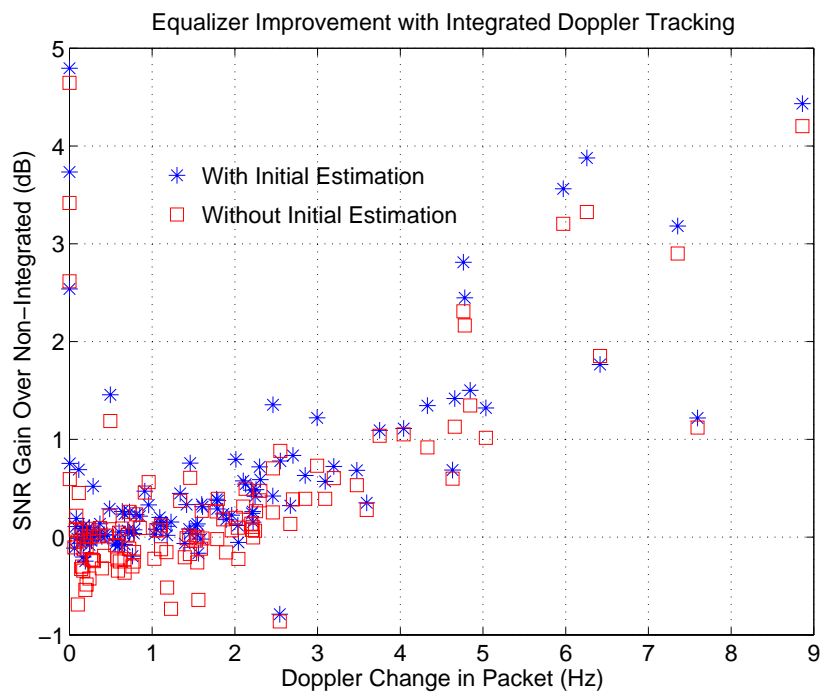
Fig. 10.   Improvement of the Doppler tracking receiver with respect to the receiver with initial Doppler estimation and fixed resampling rate (case C).
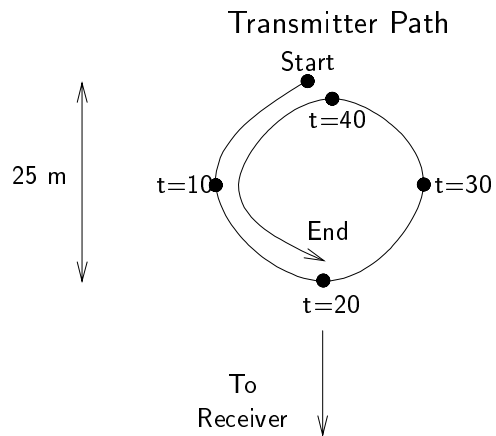
Fig. 11. Path of small boat while transmiting a 60 s continuous signal for Doppler change test (Case D).
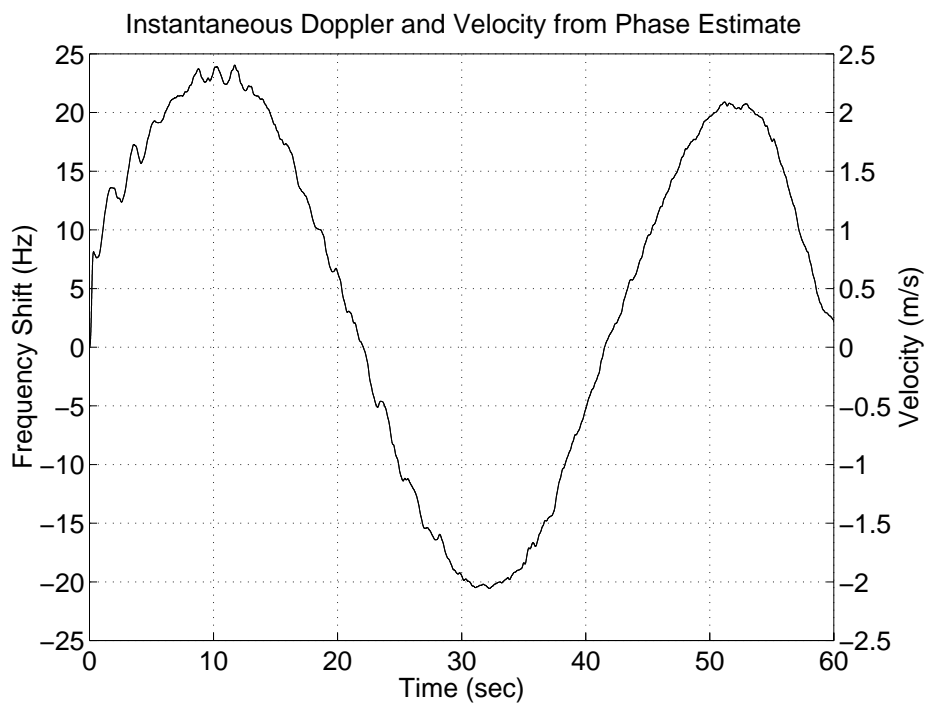
Fig. 12. Doppler frequency shift and resulting relative source-receiver velocity while the source follows the track in Fig. 11.